Determination of the Lamellar Phase Content in MCM-41 Using X-ray Diffraction, Nitrogen Adsorption, and Thermogravimetry

Michal Kruk and Mietek Jaroniec*

Department of Chemistry, Kent State University, Kent, Ohio 44242

Yong Yang and Abdelhamid Sayari*

Department of Chemical Engineering and CERPIC, Université Laval Ste-Foy, Québec, Canada G1K 7P4

Received: September 24, 1999; In Final Form: December 8, 1999

Self-consistent approaches for quantification of the phase composition of ordered mesoporous materials (OMMs) are proposed on the basis of powder X-ray diffraction (XRD), and, for the first time, on the basis of gas adsorption and thermogravimetry (TGA). A series of hexagonal MCM-41 samples containing different amounts of the lamellar phase was synthesized and characterized using XRD, nitrogen adsorption, and high-resolution TGA. To quantify the phase composition of these samples, pure hexagonal and lamellar materials with appropriate structural properties were prepared, and used to calibrate the quantitative XRD analysis and to develop a new methodology for the phase-composition determination on the basis of gas adsorption and TGA. The phase-composition determination from gas adsorption data was based on the mutual independence of adsorption on different components of mixtures. The relative amounts of components of the mixed phases were obtained by fitting the adsorption isotherms measured on the calcined mixed phase materials with those measured on calcined pure hexagonal and lamellar phases. The resulting fits were remarkably good in the entire pressure range on both adsorption and desorption branches of the isotherms. The TGA quantification of the lamellar phase content was possible because of pronounced differences in the weight loss temperature ranges for hexagonal and lamellar components of the mixed phases. The results of the three methods proposed herein were in a good agreement with one another, and thus these methods were validated for independent use. Moreover, from their very nature, these methods promise to be applicable for determination of the phase composition of other mixed OMM phases.

1. Introduction

Ordered mesoporous materials (OMMs)[1,2] currently attract considerable attention because of their tailored structures and compositions, which make them suitable for a wide variety of applications in catalysis, environmental cleanup, solid-phase extraction, and advanced materials design.[3−14] Determination of the phase purity is an important problem in characterization of OMMs,[13,15−18] because their synthesis often involves various phase transitions,[19−30] and thus mixtures of different ordered phases may be obtained instead of pure phases. There is also a possibility of contamination of the OMM phase with an amorphous phase.[31,32] Therefore, it is important to develop proper methods for qualitative and quantitative determination of phase composition of OMMs.

Detection of different OMM phases can readily be achieved using powder X-ray diffraction, because different ordered phases exhibit distinct XRD spectra.[1−13] However, quantification of the content of different OMM phases using XRD[33] is expected to be difficult, since it is well-known (see, for instance, ref 18 and references therein) that the same type of OMM phase may exhibit a different degree of the structural ordering as well as different unit cell size and pore wall thickness. Consequently, the position and intensity of XRD reflections may vary widely, making calibration of the XRD analysis difficult, and limiting the range of samples for which a given calibration would be suitable. Therefore, only rarely have the results of XRD estimations of the phase composition of OMMs been reported.[25,26] In one of these studies,[25] the characterization procedure was not described sufficiently to determine whether the results were quantitative or merely qualitative, and the results were not compared with those from independent experimental methods. In the second study,[26] it was stated that the determination of the phase composition was only qualitative because of the lack of suitable calibration.

Phase composition of OMMs can also be examined using transmission electron microscopy (TEM).[15−17] However, interpretation of TEM data is not unambiguous because of the many possible alignments of the OMM specimens with respect to the direction of the electron beam.[17] For instance, the MCM-41 phase[1] may produce images identical to those of a lamellar phase when imaged perpendicular to the channels or may give rise to rather featureless TEM images, when the MCM-41 channels are neither parallel nor perpendicular to the direction of the electron beam. [17] Gas adsorption is another technique which was used to elucidate the phase composition of OMMs.[32,34] However, these estimations were based on the comparison of the amount adsorbed, pore volume, or specific surface area for different OMM samples. In general, these structural properties may vary widely for the same kind of OMM material and are functions of the unit cell size and pore wall thickness (in the case of phase-pure samples of a given type of the framework

* Corresponding authors. E-mail, jaroniec@columbo.kent.edu; phone, (330) 672-3790; fax, (330) 672-3816. E-mail, sayari@gch.ulaval.ca; phone, (418) 656-3563; fax, (418) 656-5993.

10.1021/jp993419o CCC: $19.00
Published on Web 02/02/2000

composition).[18,35] So, the comparison of these structural properties is not likely to provide a reliable basis of the phase-content evaluation unless the compared materials have the same unit cell dimension and pore wall thickness, not to mention a similar framework composition. An attempt was also made to estimate the phase content in MCM-41 on the basis of the thermogravimetric weight loss in the temperature range corresponding to the surfactant decomposition.[32] However, the surfactant content in a given OMM may vary, depending, for instance, on the pore wall thickness,[36] and the possibly present mesostructured impurities may not be accounted for, so this method of phase-content determination may be grossly inaccurate. Another approach for the phase-purity determination, restricted so far to MCM-41, is to use a geometrical relation between the unit cell parameter, pore size, pore volume, and the content of the MCM-41 phase.[18]

It can be concluded that there has been no satisfactory methodology for evaluation of the phase composition of OMMs, although elaboration of such a methodology is strongly needed. One obvious choice for the method to be used is XRD, and the major challenge lies in calibration of this technique to make it suitable for a particular kind of determination. Gas adsorption is also highly promising, because the overall adsorption for a given sample is a sum of the amounts adsorbed on the phases, which constitute the sample.[37] This offers a clear way to calculate the phase composition, provided adsorption behaviors of pure components of the sample can be accurately determined and are distinctly different from one another. To this end, it has been demonstrated recently that nitrogen adsorption isotherms for good-quality MCM-41, MCM-48, and SBA-1 are different and can readily be distinguished.[38]

Another promising technique is thermal analysis, because different OMMs prepared under very similar conditions were shown to exhibit different weight changes associated with the surfactant decomposition,[22] and the thermogravimetric behavior of OMMs was shown to be strongly dependent on their framework composition.[1,39−41] TGA was also reported to provide information about surfactant/expander organization in amine-expanded mesoporous silicas.[42] Thus, it is worthwhile to verify whether different OMM phases have distinct thermogravimetric behaviors, which would open up an opportunity for their quantification on the basis of the weight change patterns.

The aim of the current study was to develop methods for determination of the phase composition of mixtures of hexagonal MCM-41 and lamellar phases. MCM-41 is a prominent member of the OMM family,[1,3−14] whereas the lamellar phase is a common mesostructured phase,[1,3−9,12,13,19−30,43−47] which is often formed at certain stages of the OMM synthesis.[19−30] The lamellar phase collapses upon calcination[1] and thus is a common amorphous impurity in calcined OMMs. The methodology for determination of the phase composition of the MCM-41/lamellar mixtures using XRD, gas adsorption, and TGA was successfully developed, and the results from different methods were found to be consistent. The elaborated methods have different accuracy, complexity, and range of applicability, and it is expected that they can be used independently or can complement one another.

2. Materials and Methods

2.1. Materials. The synthesis of pure hexagonal MCM-41 phase (denoted as H) and mixed hexagonal−lamellar phases (HL) was carried out using the synthesis gel composition reported by Janicke et al.[48] The overall composition was 1 SiO_2: 0.088 TMA^+: 0.32 CTMABr: 0.0036 Na_2O: 63.3 H_2O, where TMA^+ denotes tetramethylammonium cations and CTMABr denotes cetyltrimethylammonium bromide. Typically, 2.09 g of sodium silicate (14 wt % NaOH, 27 wt % SiO_2) was added to 4.47 g of tetramethylammonium silicate (10 wt % SiO_2) under stirring. Then, a mixture of 1.53 g of Cab-O-Sil M-5 and 9.87 g of water was added. After about 30 min of stirring, a solution with 4.93 g of CTMABr in 33.34 g of water was added to the above mixture. The gel was aged for 1 h under stirring, then transferred into a Teflon-lined autoclave and heated statically, first at 353 K for 48 h and then at 423 K for different periods of time. The obtained material was separated by filtration, washed thoroughly with distilled water, and dried overnight under ambient conditions.

The samples obtained after 24, 26, 30, 36, and 48 h of heating at 423 K will be referred to as H, HL1, HL2, HL3, and HL4, respectively. Calcination was performed first at 813 K (this temperature was reached using a heating rate of 2 K/min) in flowing nitrogen for 1 h, and subsequently in air for 3 h. It should be noted that hydrothermal synthesis of OMMs at high temperatures (about 423 K) was often reported to involve various phase transformations and unit-cell enlargement phenomena (see ref 14 and references therein). In the case of the high-temperature synthesis applied here, the partial transformation from the hexagonal to the lamellar phase was sometimes accompanied by a pore size enlargement (up to about 4.9 nm), similarly to the unit-cell expansion procedures reported in the literature.[14,49−53] Because the current study was focused on the quantification of the phase composition, in which case the similarity of the properties of H and L phases in different samples is important, these materials with enlarged unit cells will not be considered.

The pure lamellar phase (L) was prepared using the synthesis gel composition and conditions reported by Cheng et al.[25] The overall synthesis gel composition was 1 SiO_2: 0.317 TMAOH: 0.45 CTMABr: 67 H_2O. CTMABr (5.466 g) was added under stirring to a solution of 3.848 g of tetramethylammonium hydroxide (TMAOH, 25 wt %) in 37.1 g of water. After 15 min, 2 g of Cab-O-Sil M-5 silica were added to this mixture, followed by 30 min of stirring. The mixture was then loaded into a Teflon-lined autoclave and heated under autogenous pressure at 423 K for 40 h. Separation, drying, and calcination of the product were carried out as described above.

2.2. Measurements. Powder X-ray diffraction spectra were acquired on a Siemens D5000 diffractometer using nickel-filtered copper Kα radiation. Nitrogen adsorption measurements were carried out on an ASAP 2010 volumetric adsorption analyzer (Micromeritics, Norcross, GA). Before the adsorption measurements, the calcined samples were degassed under vacuum at 473 K for about 2 h, whereas the uncalcined materials were degassed at room temperature until vacuum of about 5 μm Hg was reached, which usually took between 2 and 10 h. Weight loss curves were recorded under nitrogen flow on a high-resolution TGA 2950 thermogravimetric analyzer (TA Instruments, New Castle, DE). The high-resolution mode, with a maximum heating rate of 5 K min^{-1}, was used. The sample size was about 10 mg.

2.3. Methods. The quantitative XRD analysis was carried out using a doping method.[33] An uncalcined sample containing both hexagonal and lamellar phases was mixed with a given amount of the uncalcined pure lamellar or pure hexagonal phase of essentially the same properties (such as the interplanar spacing, and the primary mesopore size in the case of the H phase). The doped sample was carefully mixed to attain the required homogeneity, and its XRD pattern was recorded. The

content of the doped phase was evaluated on the basis of the change in the ratio of areas of the XRD peaks corresponding to the H and L phases. Calculation of the relative amount of the hexagonal or lamellar phases, denoted $x_N(H)$ and $x_N(L)$, respectively, was carried out by solving simultaneously eqs 1 and 2 or eqs 1 and 3, respectively.

$$\frac{x_N(H)}{x_N(L)} = kR_{(HL)} \quad (1)$$

$$\frac{x_N(H) + m}{x_N(L)} = kR_{(HL+H)} \quad (2)$$

$$\frac{x_N(H)}{x_N(L) + n} = kR_{(HL+L)} \quad (3)$$

where $x_N(H)$ and $x_N(L)$ are the weight fractions of the uncalcined hexagonal and lamellar phases in the HL material, respectively; $R_{(HL)}$, $R_{(HL + H)}$, and $R_{(HL + L)}$ stand for the ratios of the (100) XRD peak area for the hexagonal phase and the (001) peak area for the lamellar phase in the HL materials and in the HL materials doped with the given amount of the pure hexagonal (H) or pure lamellar (L) phase; k is a constant; and m and n are the weight ratios of the added H or L pure phase, respectively, to the HL phase in the mixed samples used for XRD analysis.

The BET specific surface area, S_{BET}, was evaluated using nitrogen adsorption data in a relative pressure, p/p_0 (where p is the equilibrium vapor pressure and p_0 is the saturation vapor pressure), range from 0.04 to 0.2.[54] The total pore volume, V_t, was calculated on the basis of the amount adsorbed at a relative pressure of about 0.99.[54] The primary mesopore volume (V_p) and the external surface area (S_{ex}) were evaluated by the α_s plot method[52,54] using the standard reduced adsorption (α_s) range from 1.4 to 1.8, whereas the micropore volume was calculated using the α_s range from 0.4 to 0.7. A macroporous silica LiChrospher Si-1000 was used as a reference adsorbent.[52,55] The primary mesopore size, w_d, of the calcined MCM-41 was calculated using the following equation based on the geometrical model of a honeycomb structure:[56, 57]

$$w_d = cd_{100}\left(\frac{\rho V_p}{1 + \rho V_p}\right)^{1/2} \quad (4)$$

where d_{100} is the (100) interplanar spacing of the calcined sample determined using XRD, ρ is the pore wall density (assumed to be 2.2 g cm^{-3}), and c is a constant dependent on the pore geometry. The constant c is equal to 1.213 for circular and hexagonal pore geometry (for the latter, the pore diameter is defined as the diameter of a circle with area equal to that of the hexagonal pore cross section). Detailed discussion of this calculation procedure can be found elsewhere.[18] Pore-size distributions for the samples under study were evaluated using the equation for the pore size as a function of the capillary condensation pressure and the statistical film thickness curve, both derived using Kruk−Jaroniec−Sayari (KJS) method.[58] This method employs ordered mesoporous materials of known pore sizes determined using independent experimental techniques, for instance MCM-41 silicas characterized by eq 4[58] or modified MCM-41 samples,[59] to calibrate the pore size analysis on the basis of gas adsorption data. Equations developed from such calibration procedures can easily be employed in various algorithms for calculation of the pore size distribution, for instance in the Barrett−Joyner−Halenda (BJH)[60] procedure. In the current study, the KJS relations for pure-silica materials with cylindrical pores were used[58] and the BJH procedure was employed. The primary mesopore size, w_{KJS}, is defined as the maximum of the KJS pore size distribution.

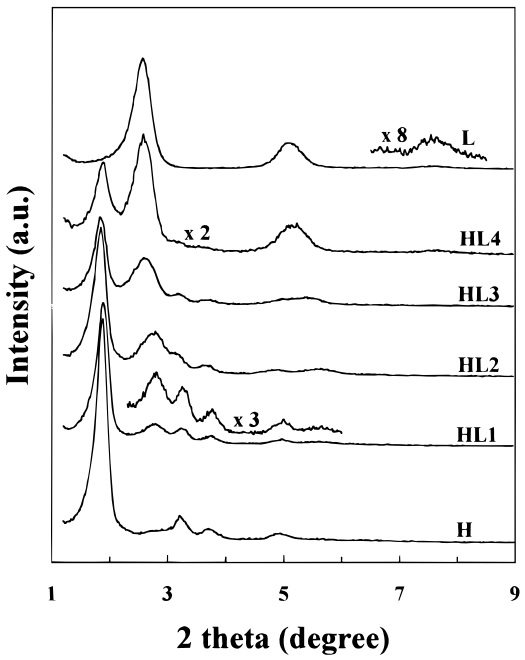

Figure 1. Powder X-ray diffraction spectra for the uncalcined samples.

TABLE 1: X-ray Diffraction Interplanar Spacing for the Samples under Study[a]

sample	d_{100}^N(H) (nm)	d_{001}^N(L) (nm)	d_{100} (nm)
H	4.70		4.50
HL1	4.65	3.15	4.46
HL2	4.75	3.15	4.65
HL3	4.75	3.40	4.50
HL4	4.64	3.40	4.90
L		3.42	

[a] d_{100}^N(H) and d_{001}^N(L) are the (100) and (001) interplanar spacings for the uncalcined hexagonal and lamellar phases, respectively; d_{100} is the (100) interplanar spacing for the calcined hexagonal phase.

3. Results and Discussion

3.1. X-ray Diffraction. Powder XRD spectra for uncalcined samples under study are shown in Figure 1. The XRD pattern for sample H featured four well-resolved peaks characteristic of the good-quality hexagonal MCM-41 phase.[1] The XRD patterns for the HL samples exhibited not only peaks related to the presence of the hexagonal phase, but also a series of the (00l) reflections (l = 1, 2 or l = 1, 2, 3) typical of a lamellar phase.[1] Therefore, it is inferred that the HL samples are mixtures of hexagonal and lamellar phases. As the synthesis time at 423 K increased from 26 to 48 h, the intensity of the peaks characteristic of the hexagonal phase gradually decreased in comparison to the intensity of the lamellar phase peaks. This indicates that the weight ratio of the lamellar to the hexagonal phase in the samples increased in the order from HL1 to HL4. However, on the basis of these XRD spectra alone, it is rather difficult to exclude the possibility of the occurrence of an amorphous phase. Moreover, the quantification of the phase composition from these XRD spectra is difficult without a proper calibration.

The values of the (100) interplanar spacing for the hexagonal phase and the (001) interplanar spacing for the lamellar phase are listed in Table 1. It is interesting to notice that both the d_{100} and d_{001} interplanar spacings for the hexagonal and lamellar

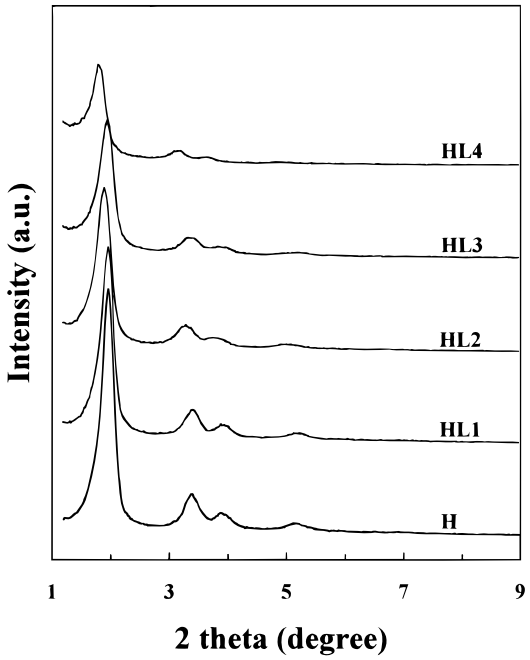

Figure 2. Powder X-ray diffraction spectra for the calcined samples.

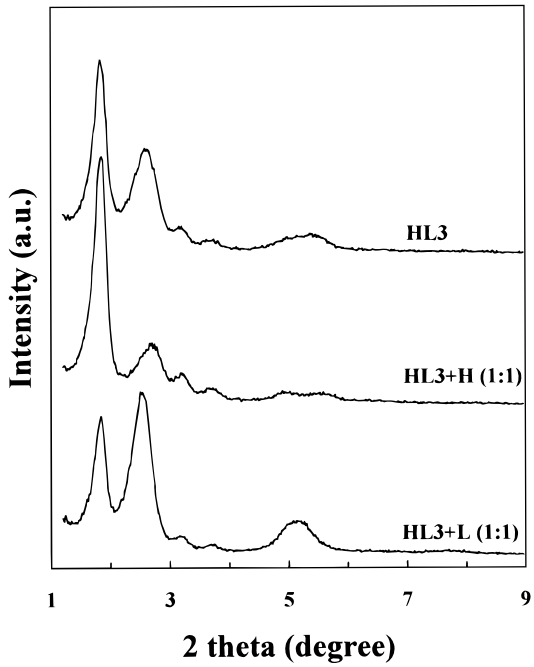

Figure 3. Representative powder X-ray diffraction spectra for the uncalcined HL3 material and its mixtures with the uncalcined pure hexagonal (H) or lamellar (L) phases.

phases were hardly affected by the sample composition. As expected, upon calcination, only the XRD peaks corresponding to the hexagonal phase persisted (Figure 2). The d_{100} interplanar spacings for the calcined samples are listed in Table 1.

To evaluate the phase composition of the materials under study using quantitative XRD methods, a proper calibration is required. To carry out such a calibration, one needs pure hexagonal and lamellar phases with properties essentially the same as those of the components of the HL materials. Uncalcined sample H can be used as a pure hexagonal phase, since its d_{100} interplanar spacing and other properties (as will be demonstrated later) were highly similar to those of the hexagonal phases in the uncalcined HL samples. However, the procedure used for the synthesis of H and HL samples was found to be unsuitable for the preparation of a pure lamellar phase, because the obtained materials always had some residual hexagonal domains even if the synthesis time at 423 K was extended to 2 weeks. So, the pure lamellar phase was prepared using the same surfactant template and temperature of the final hydrothermal treatment step, but a different synthesis procedure.[25] The XRD spectrum of the L phase is shown in Figure 1. The d_{001} interplanar spacing of the pure L phase was found to be similar to those of the lamellar phases in the HL samples (see Table 1). The similarity of these phases was further confirmed using nitrogen adsorption and thermogravimetry, as will be shown later. As expected, the XRD spectrum of the L phase became featureless after calcination, confirming the layered nature of this silicate−surfactant material.

After having obtained suitable pure hexagonal and lamellar phases, a quantitative XRD determination of the phase composition of these materials became possible. Illustrative XRD spectra for mixtures of the HL samples with pure L or with pure H phases are shown in Figure 3, and phase contents determined on the basis of these spectra are listed in Table 2. It can be seen that the sums of contents of the H and L phases were quite close to 100% (102−123%), suggesting that no appreciable amounts of an amorphous silica phase occurred in the HL materials. The fact that the sums of the determined phase contents somewhat exceeded 100% may be related to the inherent difficulty in XRD quantification of phase composition

TABLE 2: Results of the Quantitative X-ray Diffraction Analysis[a]

sample	weight ratio	intensity ratio I_{100}/I_{001}	x_N^{XRD} (%)
HL1		7.51	
HL1 + L	2:1	2.17	20 (L)
HL2		3.04	
HL2 + H	1:1	6.85	80 (H)
HL2 + L	1:1	0.92	43 (L)
HL3		1.45	
HL3 + H	1:1	3.99	57 (H)
HL3 + L	1:1	0.52	56 (L)
HL4		0.55	
HL4 + H	2:1	1.55	28 (H)
HL4 + L	1:1	0.24	74 (L)

[a] Weight ratio: weight ratio used in the preparation of mixed samples; intensity ratio: ratio of areas of the (100) and (001) peaks of the uncalcined hexagonal and the lamellar phases, respectively; x_N^{XRD}: weight percentage of the hexagonal (H) and lamellar (L) phases in uncalcined samples as determined based on XRD data.

for materials with noncrystalline pore walls. Further studies will be required to assess whether the consistency of the XRD quantification can be further improved. Anyway, it is clear from the obtained results that the HL samples under study exhibited a wide range of phase compositions from predominantly hexagonal to essentially lamellar. Thus, this series of materials can be considered as suitable for thorough verification or calibration of other quantitative methods to evaluate the phase composition of hexagonal/lamellar mixtures.

3.2. Nitrogen Adsorption. General Characteristics of the Samples. Nitrogen adsorption isotherms for the samples under study are shown in Figures 4 and 5, and results of calculations carried out on their basis are listed in Table 3. It can be seen that an adsorption isotherm for the calcined pure hexagonal phase exhibited a narrow, triangular hysteresis loop at relative pressures between 0.4 and 0.45, with a capillary condensation step at a relative pressure of about 0.42. Similar hysteresis loops were previously observed for MCM-41 with comparable pore sizes.[58] At higher relative pressures, the adsorption isotherm was relatively flat and the desorption branch essentially followed

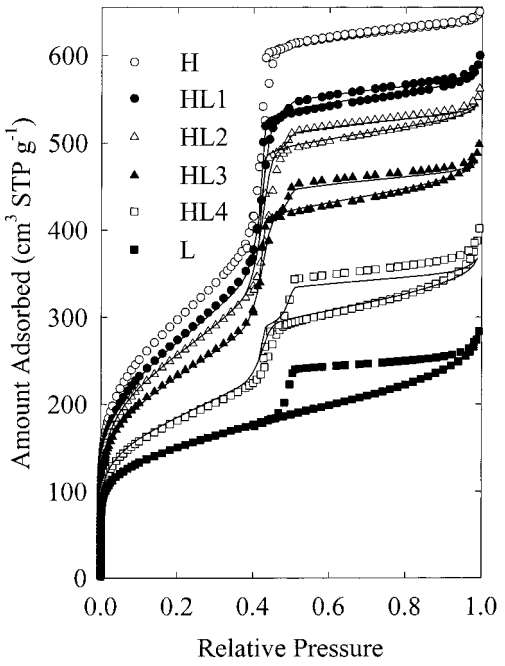

Figure 4. Nitrogen adsorption isotherms for the calcined hexagonal (H), lamellar (L), and hexagonal−lamellar (HL) samples. Symbols show the experimental data points, whereas lines provide results of fitting these points with a linear combination of experimental data for the calcined pure H and L phases. In the case of HL1−HL3, it was assumed that the sum of contents of the H and L phases is 100%, whereas in the case of HL4, no restrictions were imposed on the solution of the fitting procedure.

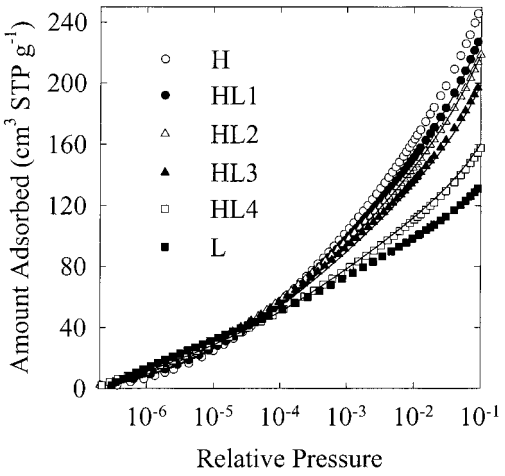

Figure 5. Low-pressure nitrogen adsorption isotherms for the calcined hexagonal (H), lamellar (L), and HL materials. Notation is the same as in Figure 4.

the adsorption branch. The increase in the amount adsorbed at pressures close to the saturation vapor pressure was rather small, and thus it can be concluded that the adsorption on the external surface of the calcined pure H phase proceeded essentially via multilayer adsorption rather than capillary condensation. This in turn indicates that the capillary condensation in interparticle pores of this material did not take place in the pressure range attainable by our adsorption equipment, and thus these pores were relatively large (the application of the Kelvin equation[54,58] allows one to estimate that their size was above 200−400 nm).

In contrast to the adsorption on the calcined pure hexagonal phase, the adsorption isotherm for the calcined pure lamellar phase exhibited no step on its adsorption branch, indicating a highly nonuniform porous system. A pronounced, broad, triangular hysteresis loop was observed at relative pressures above ca. 0.4. It is also interesting to note that the calcined L phase had a quite considerable BET specific surface area and total pore volume (about 500 m^2 g^{-1} and 0.42 cm^3 g^{-1}, respectively). As can be seen in Figure 6, the comparative plot for the H phase exhibited excellent linearity in the low-pressure range (that is for low α_s values), whereas the comparative plot of the L phase exhibited a highly nonlinear behavior, indicating the presence of microporosity. The corresponding micropore volume is listed in Table 3. Mesopore size distributions (PSDs) for the calcined pure H and L phases were also dramatically different: the H phase exhibited a sharp peak on its PSD, whereas the PSD of the L phase was extremely broad and without a well-pronounced maximum (see Figure 7). Nitrogen adsorption isotherms for all of the calcined HL phases exhibited hysteresis loops with sharp capillary condensation/evaporation steps in the relative pressure range from 0.4 to 0.46, resembling the adsorption isotherm for the calcined H phase (Figures 4 and 5). In addition, wide, triangular hysteresis loops were observed at relative pressures above about 0.48, which resembled the adsorption behavior of the pure lamellar phase. The extent to which the latter hysteresis loop was pronounced for the HL materials was clearly correlated with the contents of the L phase in the samples, as determined using XRD. It should be noted that a nitrogen adsorption isotherm with a similar wide, triangular, high-pressure hysteresis loop was reported for a mixed MCM-48/lamellar silica,[30] which indicates that collapse of the lamellar phase in different types of mixed phases may give rise to highly similar adsorption properties.

To determine whether the observed adsorption behavior of the calcined L phase resulted from the structure of its particles in the uncalcined material or from the collapse upon calcination, nitrogen adsorption measurement was performed for the uncalcined L sample. It turned out that this silicate−surfactant composite was essentially nonporous and that its specific surface area was below 10 m^2 g^{-1}, so it can be concluded that the porosity of the calcined L phase formed as a result of collapse of the ordered layered structure upon removal of the surfactant template. However, it needs to be kept in mind that the presence of a pronounced high-pressure hysteresis is not always an evidence of collapse of some layered phases. For instance, wide rectangular hysteresis loops were observed both for highly ordered uncalcined and calcined MCM-41 silicas prepared using the pH adjustment method.[61] The uncalcined hexagonal phase also exhibited a very low specific surface area (below 10 m^2 g^{-1}). It was especially interesting to examine the low-pressure nitrogen adsorption data for the H and L samples, because it was recently demonstrated[61] that uncalcined hexagonal MCM-41 materials exhibit relatively hydrophobic surface properties resembling those of polymeric alkylsilyl-modified silicas.[59,62] This behavior was attributed to the presence of electrostatically bonded surfactant molecules on the external surface of these materials.[61] It turned out that low-pressure nitrogen adsorption data for the samples investigated here also clearly indicated hydrophobic surface properties. This suggests that the presence of electrostatically bonded surfactant on the external surface of the silicate/surfactant composites may be a general feature of such materials, at least those prepared via synthesis pathways involving direct electrostatic attraction between the surfactant ions and inorganic ionic species of the opposite charge.

3.3. Quantitative Determination of the Phase Composition from Gas Adsorption Data. As discussed above, nitrogen adsorption properties of the calcined HL phases under study gradually evolved from those of the calcined pure hexagonal phase to those of the calcined pure lamellar phase (see Figures

TABLE 3: Pore Structure Properties of the Calcined Samples under Study, Determined on the Basis of Nitrogen Adsorption and Adsorption/XRD Data[a]

sample	S_{BET} (m^2 g^{-1})	V_t (cm^3 g^{-1})	S_{ex} (m^2 g^{-1})	V_p (cm^3 g^{-1})	V_{mi} (cm^3 g^{-1})	w_d (nm)	w_{KJS} (nm)
H	1080	1.00	50	0.93	0.00	4.47	4.33
HL1	990	0.91	90	0.78	0.01	4.30	4.30
HL2	930	0.85	100	0.70	0.02	4.40	4.45
HL3	840	0.76	120	0.56	0.03	4.06	4.30
HL4	650	0.60	160	0.34	0.04	3.87	4.45
L	530	0.42	170	0.15	0.05		[b]

[a] S_{BET}, BET specific surface area; V_t, total pore volume; S_{ex}, external surface area; V_p, primary mesopore volume; V_{mi}, micropore volume; w_d, MCM-41 primary mesopore diameter evaluated using eq 4; w_{KJS}, primary mesopore diameter evaluated using the BJH algorithm with KJS calibration. [b] Broad pore size distribution, so w_{KJS} cannot accurately be determined.

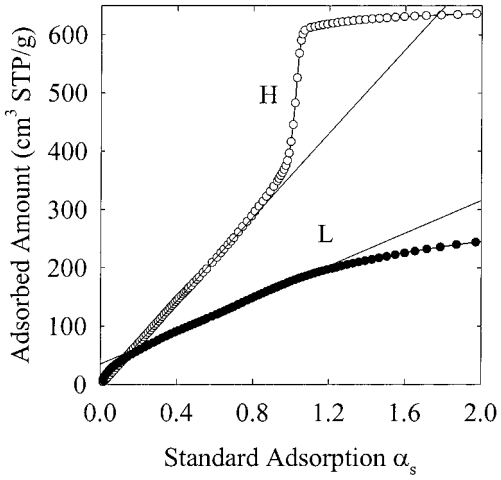

Figure 6. α_s plots for the calcined pure hexagonal (H) and pure lamellar (L) phases.

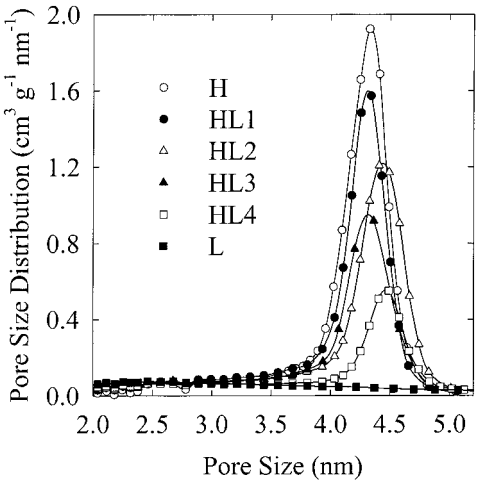

Figure 7. Mesopore size distributions for the calcined samples under study.

4 and 5). This is not surprising, because adsorption behavior of the mixtures of different phases is a combination of adsorption behaviors of the components, provided there is no mutual influence of each of these components on porous structures, pore accessibility, or surface properties of the other components. In the case of the HL materials under study, one can expect that there is no such influence, so adsorption properties of the phases constituting the samples are mutually independent and the overall adsorption is simply the sum of adsorption on the different phases. This clearly opens up an opportunity for quantification of the phase composition on the basis of adsorption data. Therefore, the adsorption isotherms, $v_{HL}(p/p_0)$, for the calcined HL phases were fitted with linear combinations of adsorption isotherms for the calcined H phase, $v_H(p/p_0)$, and

TABLE 4: Results of the Quantitative Determination of the Phase Composition using Nitrogen Adsorption[a]

sample	x_C^{A1}(H) (%)	x_C^{A1}(L) (%)	x_C^{A2}(H) (%)	x_C^{A2}(L) (%)
HL1	82 (81)	18 (19)	80 (80)	23 (23)
HL2	73 (71)	27 (29)	71 (70)	31 (31)
HL3	55 (52)	45 (48)	52 (50)	54 (53)
HL4	25 (20)[b]	75 (80)	28 (25)[b]	68 (67)

[a] x_C^{A1}(H) and x_C^{A1}(L), weight percents of the calcined hexagonal and lamellar phases, respectively, determined under the assumption that $x_C^{A1}(H) + x_C^{A1}(L) = 100\%$; x_C^{A2}(H) and x_C^{A2}(L), weight percents of the calcined hexagonal and lamellar phases, respectively, determined without the latter assumption. Data in parentheses were obtained using another lamellar phase prepared in the same conditions. [b] For explanation, see text.

the calcined L phase, $v_L(p/p_0)$:

$$v_{HL}(p/p_0) \text{ fitted with } x_C^{Ai}(H)v_H(p/p_0) + x_C^{Ai}(L)v_L(p/p_0) \quad (5)$$

where x_C^{Ai}(H) and x_C^{Ai}(L) are fitting coefficients. The adsorption isotherms for the samples under study were interpolated on the same vector of relative pressures, and the fitting was carried out using the least-squares method. Two different types of calculations were performed. First, it was assumed that (1) the H and L phase components of the calcined HL phases have essentially identical adsorption properties as those of the calcined pure H and L samples, and (2) the HL samples are composed of H and L phases only. In this case, the fitting coefficients correspond to the weight fractions of the phases in the calcined HL samples, and their sum is equal to 100% (in this work, we shall express the weight fractions in weight percents). The results of fitting under these assumptions are provided in Table 4 (denoted using a superscript "A1") and the corresponding fits for HL1−HL3 samples are shown in Figures 4 and 5. The fits were in excellent agreement with the experimental data in the entire pressure range, including low- and high-pressure range of adsorption isotherms as well as desorption isotherms. It should be noted here that the fitting procedure was based on adsorption data only and that the points in the capillary condensation range (relative pressure between 0.37 and 0.52) were not used in calculations. The inclusion of the latter points would have a negative influence on the accuracy of the fitting procedure, because sharp capillary condensation steps present on the adsorption isotherms for the H and HL samples under study were centered at slightly different relative pressure values. These small differences corresponded to appreciable differences in the amounts adsorbed at a given pressure in the capillary condensation region, which would introduce some inaccuracy in the least-squares procedure.

The quality of the attained fits clearly demonstrated that the assumptions used for our calculations were correct, and thus the fitting coefficients can be regarded as the weight fractions of phases in the calcined samples under study. To further test

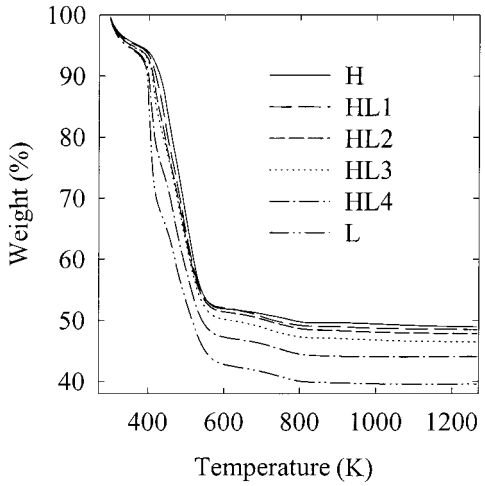

Figure 8. Thermogravimetric weight change curves for uncalcined samples.

the reliability of the fitting procedure, adsorption data for another calcined pure lamellar phase prepared under the same conditions were used in the calculations. As can be seen in Table 4, the results were found to be very similar, showing the stability and reproducibility of the results generated by the fitting procedure employed. Moreover, the fitting was also carried out without the assumption that the sum of fitting coefficients is equal to 100%. This corresponds to the following properties of the samples: (1) adsorption properties of the H and L phases in the calcined HL materials are somewhat different from those of the calcined pure H and L phases, and/or (2) there is an additional low-surface-area phase present in the samples. It should be noted that the presence of an additional high-surface-area phase would have to be accounted for explicitly in the fitting procedure, because it would have a noticeable influence on adsorption properties of the mixed-phase materials, unless its content were very low. The results of the fitting procedure without restrictions on the values of the fitting coefficients are listed in Table 4 (denoted with superscript "A2"). The fits were very good and the sums of fitting coefficients for the HL samples under study were close to 100%, which showed that the H and L components of these HL samples generally had similar adsorption properties to those of the pure H and L phases. In the case of the HL1−HL3 materials, the sums of fitting coefficients were slightly above 100%, which may indicate that the H and L components actually had slightly larger adsorption capacities than the pure H and L phases. However, in the case of HL4, the sum was below 100%, which may be attributed to the fact that the calcined hexagonal phase in this material had thicker pore walls than the hexagonal phases in other samples, since it had larger d_{100} interplanar spacing (see Table 1) and yet similar pore size (see w_{KJS} in Table 3). Because of the presence of thicker pore walls, the H component of the HL4 sample is expected to have lower adsorption capacity,[18] and thus its actual weight fraction is expected to be somewhat higher than that obtained from the fitting procedure, which from its very nature is based on the comparison of the adsorption capacities of materials. The results of the A2 fitting procedure for sample HL4 are shown in Figures 4 and 5.

3.4. Thermogravimetry. Thermogravimetric studies of the uncalcined materials revealed that their weight change patterns were markedly different and gradually evolved from those for the pure hexagonal phase to those of the pure lamellar phase. As can be seen in Figure 8, the residual weight at 1270 K gradually decreased as the lamellar phase content increased. This

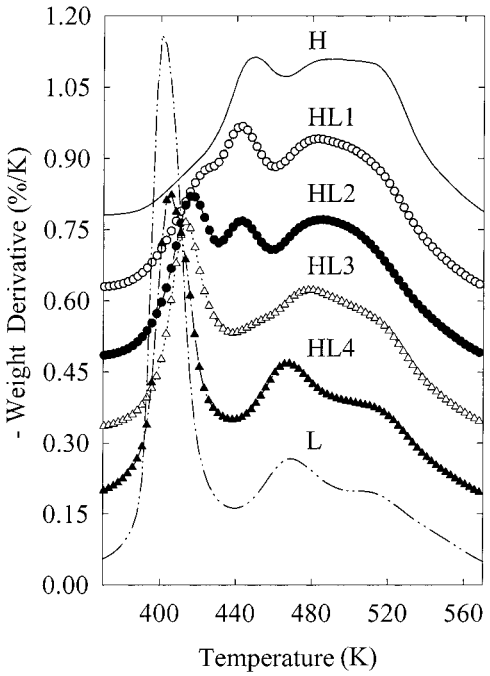

Figure 9. Thermogravimetric weight change derivatives for uncalcined samples. To facilitate the comparison, the derivative curves were shifted by 0.15, 0.3, 0.45, 0.6, and 0.75%/K for HL4, HL3, HL2, HL1, and H samples, respectively.

behavior reflected different surfactant/silica ratios in the samples under study and was similar to that observed by others for pure hexagonal and lamellar phases.[22] The value of the residue may, in principle, provide some information about the content of the hexagonal and lamellar phase, but such estimations would be very crude, lack generality, or even be misleading if the sample were contaminated with an amorphous silica. In contrast, the weight change derivatives (see Figure 9) revealed distinctly different patterns of thermogravimetric behavior for the pure lamellar and hexagonal samples, and intermediate behaviors for the HL mixtures. The weight change derivative curve for the pure hexagonal phase exhibited two coalesced peaks at about 450 and 500 K, and that for the pure lamellar phase had a prominent peak at much lower temperatures (about 400 K) and two weaker and often poorly separated peaks at about 470 and 510 K. The HL1 phase of a relatively low content of the lamellar phase exhibited a weight change pattern characteristic of the hexagonal phase and an additional pronounced shoulder at a lower temperature (about 425 K). As the content of the lamellar phase increased, the peaks characteristic of the hexagonal phase gradually disappeared, and the low-temperature peak characteristic of the lamellar phase increased in intensity and its maximum shifted toward lower temperature. It should be noted here that the actual position and intensity of the peaks on the weight change derivatives depends to some extent on the experimental conditions. Thermogravimetric measurements reported here are inherently nonequilibrium ones, and therefore the heating rate, application of nonconstant controlled heating ramp, sample size, flow rate of gas used, and so forth, have some influence on the results. For instance, the height of peaks on the weight loss derivatives or even the presence or absence of weak peaks as well as temperatures of the peak maxima may be affected. In contrast, the weight changes corresponding to temperatures between two minima on the derivative curves are relatively well-reproducible despite the fact that their position may shift to some extent depending on the experimental conditions. Therefore, to determine the lamellar phase content,

TABLE 5: Thermogravimetric Phase-Content Analysis Data and Their Comparison with Results from the Combined Nitrogen Adsorption/TGA Analysis[a]

sample	*R* (%)	*P* (%)	*Y* (%/K)	$x_N^{TGA,P}$(L) (%)	$x_N^{TGA,Y}$(L) (%)	x_N^{A1}(L) (%)	x_N^{A1}(H) (%)
HL1	48	7.2[b]	0.28[b]	26	24	21	79
HL2	48	11.4	0.37	41	32	32	68
HL3	46	14.5	0.47	52	40	50	50
HL4	44	20.1	0.68	72	58	78	22
L	40	28.0	1.17				

[a] *R*, residue at 1270 K; *P*, weight loss corresponding to the low-temperature (about 405 K) peak on differential TGA curves; *Y*, height of the low-temperature DTGA peak; $x_N^{TGA,P}$(L), weight percentage of the lamellar phase in uncalcined sample determined on the basis of the weight loss corresponding to the low-temperature DTGA peak; $x_N^{TGA,Y}$(L), weight percentage of the lamellar phase in uncalcined sample determined on the basis of the height of the low-temperature DTGA peak; x_N^{A1}(L) and x_N^{A1}(H), weight percentages of the lamellar and hexagonal phases (in uncalcined HL materials), respectively, evaluated on the basis of the TGA residues and weight percentages obtained from nitrogen adsorption for the calcined samples (x_N^{A1}(L) and x_N^{A1}(H)). [b] There was a shoulder rather than a distinct peak in the low-temperature range on the DTGA curve, so the values corresponding to the shoulder were used.

we attempted to use the weight losses in the temperature range between the minima preceding and following the most distinct and clearly pronounced peak on the TGA derivatives, that is, the low-temperature peak (about 410 K) characteristic of the lamellar phase. The resulting weight losses and the corresponding estimates of the lamellar phase contents in the uncalcined materials are listed in Table 5. Similar results can be obtained if one performs quantification of the lamellar phase on the basis of the height of the low-temperature peak (see Table 5) but, as was mentioned above, these results are not well-reproducible, for instance because the use of larger sample weight tends to increase the peak height. It should be noted that the data from Table 5 were obtained for the samples of very similar weight in order to minimize this kind of error.

The reason why hexagonal and lamellar materials exhibited dramatically different thermogravimetric behavior is not fully understood. However, it is well-known that decomposition/desorption of the same kind of surfactant template may be dramatically influenced by the framework composition of materials.[1,39−41] This can be understood as an influence of differences in the basic properties of the framework siloxy groups and other framework groups on the process of Hoffmann elimination of alkylammonium to the corresponding alkene and low-molecular-weight amine.[1,63,64] This decomposition process leads not only to elimination of the electrostatic framework−template interactions but also to the formation of lower-molecular-weight decomposition products. Thus, the framework−surfactant interactions are crucial factors determining the thermogravimetric behavior.[1] It is hypothesized that the siloxy groups of the lamellar phase may be more strongly basic than those of the hexagonal phase and thus may promote the Hoffman elimination at lower temperatures. It should be noted that differences in the arrangement of surfactant and silicate moieties in the ordered structures of the hexagonal and lamellar phases and the effect of structural changes in the silicate framework of the lamellar phase resulting from the collapse upon heat treatment may also have some influence on the thermogravimetric behavior of the materials under study.

3.5. Comparison of Phase-Content Estimations Using Different Methods. To be able to compare the data from the different quantification methods described above, one needs to express the results as the mass of either the uncalcined or the calcined materials. It is important because the content of silica in uncalcined hexagonal and lamellar phases is significantly different, as seen from the values of the TGA residue (which is essentially the silica content in an uncalcined sample; see Table 5). Because the XRD and TGA data provide the contents of phases in uncalcined materials, the adsorption data were recalculated using the aforementioned residue values to obtain weight percentages for the uncalcined materials using the following formulas:

$$x_N(\mathrm{H}) = \left(1 + \frac{x_C(\mathrm{L})R(\mathrm{H})}{x_C(\mathrm{H})R(\mathrm{L})}\right)^{-1} \quad (6)$$

$$x_N(\mathrm{L}) = \left(1 + \frac{x_C(\mathrm{H})R(\mathrm{L})}{x_C(\mathrm{L})R(\mathrm{H})}\right)^{-1} \quad (7)$$

where $x_N(Z)$ and $x_C(Z)$ denote the weight fractions of a phase Z in the uncalcined and calcined material, respectively, whereas $R(Z)$ denotes the TGA residue (Z = H or L for the hexagonal or lamellar phases, respectively). The derivation of eqs 6 and 7 was based upon an assumption that the sum of the contents of the hexagonal and lamellar phases is equal to 100%. The results of the evaluation of the phase contents on the basis of adsorption data, recalculated to obtain the weight percentages for uncalcined materials, are listed in Table 5. It can be seen that the phase compositions evaluated on the basis of XRD (Table 2), TGA, and gas adsorption data are, in general in good agreement with one another, which is rather remarkable given that three completely different experimental techniques were used.

4. Conclusions

The current study demonstrated that it is possible to consistently determine the phase composition of hexagonal/lamellar phase mixtures using three independent experimental techniques, that is, powder X-ray diffraction, gas adsorption, and thermogravimetry. In all cases, initial calibration using pure phases is required, and thus the synthesis of the latter is crucial for the phase quantification. The quantitative determination of the phase composition using XRD appears to be the most laborious, because it requires preparation of mixtures of the samples under study with proper standards. Moreover, because the materials under current study do not have crystalline frameworks, the intensity of the XRD peaks is likely to depend on the unit-cell size, pore wall thickness, and possibly also some other variables, which may vary to some extent from one sample to another. Therefore, additional work involving a much wider variety of samples is needed to strengthen the foundations of this method. However, it needs to be kept in mind that XRD is the only technique of the three methods used that provides direct information about the presence or absence of particular ordered phases. Determination of the phase composition on the basis of nitrogen adsorption data can readily be achieved when adsorption data for calcined pure components are available. The phase composition can also be evaluated using TGA. This technique promises to be the most general and the least affected by differences in details of the porous structure of the samples. However, it is less accurate and allows one to determine

essentially only the content of the lamellar phase (because of the broad nature of TGA peaks for the hexagonal phase and their overlap with peaks of the lamellar phase). Moreover, it is yet to be verified whether the influence of heteroatoms in silicate framework will not modify the TGA behavior to such an extent that it will make the proposed quantification method inapplicable. It would be interesting to verify whether other types of surfactant-templated phases exhibit some distinct gas adsorption or TGA behaviors, which would make it possible to generalize the methods of the quantitative phase composition analysis proposed in the current study.

Acknowledgment. Donors of the Petroleum Research Fund administered by the American Chemical Society are acknowledged for partial support of this study. Funds were also provided by the Natural Science and Engineering Research Council of Canada and le Fonds pour la Formation de Chercheurs et l'Aide à la Recherche du Québec.

References and Notes

(1) Beck, J. S.; Vartuli, J. C.; Roth, W. J.; Leonowicz, M. E.; Kresge, C. T.; Schmitt, K. D.; Chu, C. T. W.; Olson, D. H.; Sheppard, E. W.; McCullen, S. B.; Higgins, J. B.; Schlenker, J. L. *J. Am. Chem. Soc.* **1992**, *114*, 10834.

(2) Yanagisawa, T.; Shimizu, T.; Kuroda, K.; Kato, C. *Bull. Chem. Soc. Jpn.* **1990**, *63*, 988.

(3) Raman, N. K.; Anderson, M. T.; Brinker, C. J. *Chem. Mater.* **1996**, *8*, 1682.

(4) Sayari, A. *Stud. Surf. Sci. Catal.* **1996**, *102*, 1.

(5) Sayari, A. *Chem. Mater.* **1996**, *8*, 1840.

(6) Sayari, A.; Liu, P. *Microporous Mater.* **1997**, *12*, 149.

(7) Corma, A. *Chem. Rev.* **1997**, *97*, 2373.

(8) Stucky, G. D.; Huo, Q.; Firouzi, A.; Chmelka, B. F.; Schacht, S.; Voigt-Martin, I. G.; Schuth, F. *Stud. Surf. Sci. Catal.* **1997**, *105*, 3.

(9) Linden, M.; Schacht, S.; Schuth, F.; Steel, A.; Unger, K. K. *J. Porous Mater.* **1998**, *5*, 177.

(10) Morey, M. S.; Davidson, A.; Stucky, G. D. *J. Porous Mater.* **1998**, *5*, 195.

(11) Moller, K.; Bein, T. *Chem. Mater.* **1998**, *10*, 2950.

(12) Ying, J. Y.; Mehnert, C. P.; Wong, M. S. *Angew. Chem., Int. Ed. Engl.* **1999**, *38*, 8, 56.

(13) Ciesla, U.; Schuth, F. *Microporous Mesoporous Mater.* **1999**, *27*, 131.

(14) Kruk, M.; Jaroniec, M.; Sayari, A. *J. Phys. Chem. B* **1999**, *103*, 4590.

(15) Alfredsson, V.; Keung, M.; Monnier, A.; Stucky, G. D.; Unger, K. K.; Schuth, F. *J. Chem. Soc., Chem. Commun.* **1994**, 921.

(16) Ciesla, U.; Grun, M.; Isajeva, T.; Kurganov, A. A.; Neimark, A. V.; Ravikovitch, P.; Schacht, S.; Schuth, F.; Unger, K. K. In *Access in Nanoporous Materials*; Pinnavaia, T. J., Thorpe, M. F., Eds.; Plenum: New York, 1995; p 231.

(17) Chenite, A.; Le Page, Y.; Sayari, A. *Chem. Mater.* **1995**, *7*, 1015.

(18) Kruk, M.; Jaroniec, M.; Sayari, A. *Chem. Mater.* **1999**, *11*, 492.

(19) Monnier, A.; Schuth, F.; Huo, Q.; Kumar, D.; Margolese, D.; Maxwell, R. S.; Stucky, G. D.; Krishnamurty, M.; Petroff, P.; Firouzi, A.; Janicke, M.; Chmelka, B. F. *Science* **1993**, *261*, 1299.

(20) Firouzi, A.; Kumar, D.; Bull, L. M.; Besier, T.; Sieger, P.; Huo, Q.; Walker, S. A.; Zasadzinski, J. A.; Glinka, C.; Nicol, J.; Margolese, D.; Stucky, G. D.; Chmelka, B. F. *Science* **1995**, *267*, 1138.

(21) Zhao, D.; Goldfarb, D. *J. Chem. Soc., Chem. Commun.* **1995**, 875.

(22) Zhao, D.; Goldfarb, D. *Stud. Surf. Sci. Catal.* **1995**, *97*, 181.

(23) Huo, Q.; Margolese, D. I.; Stucky, G. D. *Chem. Mater.* **1996**, *8*, 1147.

(24) Chen, X., Huang, L.; Li, Q. *J. Phys. Chem. B* **1997**, *101*, 8460.

(25) Cheng, C.-F.; Park, D. H.; Klinowski, J. *J. Chem. Soc., Faraday Trans.* **1997**, *93*, 193.

(26) Romero, A. A.; Alba, M. D.; Zhou, W.; Klinowski, J. *J. Phys. Chem. B* **1997**, *101*, 5294.

(27) Zhang, J.; Luz, Z.; Goldfarb, D. *J. Phys. Chem. B* **1997**, *101*, 7087.

(28) Luan, Z.; He, H.; Zhou, W.; Klinowski, J. *J. Chem. Soc., Faraday Trans.* **1998**, *94*, 979.

(29) Xu, J.; Luan, Z.; He, H.; Zhou, W.; Kevan, L. *Chem. Mater.* **1998**, *10*, 3690.

(30) Corma, A.; Kan, Q.; Rey, F. *Chem. Commun.* **1998**, 579.

(31) Kim, J. M.; Kim, S. K.; Ryoo, R. *Chem. Commun.* **1998**, 259.

(32) Schulz-Ekloff, G.; Rathousky, J.; Zukal, A. *Microporous Mesoporous Mater.* **1999**, *27*, 273.

(33) Zevin, L. S.; Kimmel, G. *Qualitative X-ray Diffraction*; Springer-Verlag: New York, 1995.

(34) Ortlam, A.; Rathousky, J.; Schulz-Ekloff, G.; Zukal, A. *Microporous Mater.* **1996**, *6*, 171.

(35) Fenelonov, V. B.; Romannikov, V. N.; Derevyankin, A. Yu. *Microporous Mesoporous Mater.* **1999**, *28*, 57.

(36) Di Renzo, F.; Coustel, N.; Mendiboure, M.; Cambon, H.; Fajula, F. *Stud. Surf. Sci. Catal.* **1997**, *105*, 69.

(37) Jaroniec, M.; Madey, R. *Physical Adsorption on Heterogeneous Solids*; Elsevier: Amsterdam, 1988.

(38) Kruk, M.; Jaroniec, M.; Ryoo, R.; Kim, J. M. *Chem. Mater.* **1999**, *11*, 2568.

(39) Schmidt, R.; Akporiaye, D.; Stocker, M.; Ellestad, O. H. *Stud. Surf. Sci. Catal.* **1994**, *84*, 61.

(40) Busio, M.; Janchen, J.; van Hooff, J. H. C. *Microporous Mater.* **1995**, *5*, 211.

(41) Occelli, M. L.; Biz, S.; Auroux, A.; Ray, G. J. *Microporous Mesoporous Mater.* **1998**, *26*, 193.

(42) Kruk, M.; Jaroniec, M.; Sayari, A. *Microporous Mesoporous Mater.*, in press.

(43) Huo, Q.; Margolese, D. I.; Ciesla, U.; Demuth, G. D.; Feng, P.; Gier, T. E.; Sieger, P.; Firouzi, A.; Chmelka, B. F.; Schuth, F.; Stucky, G. D. *Chem. Mater.* **1994**, *6*, 1176.

(44) Stucky, G. D.; Monnier, A.; Schuth, F.; Huo, Q.; Margolese, D.; Kumar, D.; Krishnamurty, M.; Petroff, P.; Firouzi, A.; Janicke, M.; Chmelka, B. F. *Mol. Cryst. Liq. Cryst.* **1994**, *240*, 187.

(45) Sayari, A.; Karra, V. R.; Reddy, J. S.; Moudrakovski, I. L. *Mater. Res. Soc. Symp. Proc.* **1995**, *371*, 81.

(46) Vartuli, J. C.; Schmitt, K. D.; Kresge, C. T.; Roth, W. J.; Leonowicz, M. E.; McCullen, S. B.; Hellring, S. D.; Beck, J. S.; Schlenker, J. L.; Olson, D. H.; Sheppard, E. W. *Chem. Mater.* **1994**, *6*, 2317.

(47) Gabelica, Z.; Clacens, J.-M.; Sobry, R.; Van den Bossche, G. *Stud. Surf. Sci. Catal.* **1995**, *97*, 143.

(48) Janicke, M.; Kumar, D.; Stucky, G. D.; Chmelka, B. F. *Stud. Surf. Sci. Catal.* **1994**, *84*, 243.

(49) Khushalani, D.; Kuperman, A.; Ozin, G. A.; Tanaka, K.; Garces, J.; Olken, M. M.; Coombs, N. *Adv. Mater.* **1995**, *7*, 842.

(50) Cheng, C.-F.; Zhou, W.; Park, D. H.; Klinowski, J.; Hargreaves, M.; Gladden, L. F. *J. Chem. Soc., Faraday Trans.* **1997**, *93*, 359.

(51) Corma, A.; Kan, Q.; Navarro, M. T.; Perez-Pariente, J.; Rey, F. *Chem. Mater.* **1997**, *9*, 2123.

(52) Sayari, A.; Liu, P.; Kruk, M.; Jaroniec, M. *Chem. Mater.* **1997**, *9*, 2499.

(53) Kruk, M.; Jaroniec, M.; Kim, J. M.; Ryoo, R. *Langmuir* **1999**, *15*, 5279.

(54) Sing, K. S. W.; Everett, D. H.; Haul, R. A. W.; Moscou, L.; Pierotti, R. A.; Rouquerol, J.; Siemieniewska, T. *Pure Appl. Chem.* **1985**, *57*, 603.

(55) Jaroniec, M.; Kruk, M.; Olivier, J. P. *Langmuir* **1999**, *15*, 5410.

(56) Dabadie, T.; Ayral, A.; Guizard, C.; Cot, L.; Lacan, P. *J. Mater. Chem.* **1996**, *6*, 1789.

(57) Kruk, M.; Jaroniec, M.; Sayari, A. *J. Phys. Chem. B* **1997**, *101*, 583.

(58) Kruk, M.; Jaroniec, M.; Sayari, A. *Langmuir* **1997**, *13*, 6267.

(59) Kruk, M.; Antochshuk, V.; Jaroniec, M.; Sayari, A. *J. Phys. Chem. B* **1999**, *103*, 10670.

(60) Barrett, E. P.; Joyner, L. G.; Halenda, P. P. *J. Am. Chem. Soc.* **1951**, *73*, 373.

(61) Kruk, M.; Jaroniec, M.; Sakamoto, Y.; Terasaki, O.; Ryoo, R.; Ko, C. H. *J. Phys. Chem. B* **2000**, *104*, 292.

(62) Jaroniec, C. P.; Kruk, M.; Jaroniec, M.; Sayari, A. *J. Phys. Chem. B* **1998**, *102*, 5503.

(63) Corma, A.; Fornes, V.; Navarro, M. T.; Perez-Pariente, J. *J. Catal.* **1994**, *148*, 569.

(64) Hitz, S.; Prins, R. *J. Catal.* **1997**, *168*, 194.